

Synthesis and Structure–Activity Relationships of Amide and Hydrazone Analogues of the Cannabinoid CB₁ Receptor Antagonist *N*-(Piperidinyl)-5-(4-chlorophenyl)-1-(2,4-dichlorophenyl)-4-methyl-1*H*-pyrazole-3-carboxamide (SR141716)

Ma. Elena Y. Francisco,[†] Herbert H. Seltzman,[†] Anne F. Gilliam,[†] René A. Mitchell,[†] Sharyl L. Rider,[†] Roger G. Pertwee,[‡] Lesley A. Stevenson,[‡] and Brian F. Thomas^{*,†}

Chemistry and Life Sciences, Research Triangle Institute, Research Triangle Park, North Carolina 27709, and Department of Biomedical Sciences, Institute of Medical Sciences, University of Aberdeen, Foresterhill, Aberdeen AB25 2ZD, Scotland, United Kingdom

Received October 25, 2001

Analogues of the biaryl pyrazole *N*-(piperidinyl)-5-(4-chlorophenyl)-1-(2,4-dichlorophenyl)-4-methyl-1*H*-pyrazole-3-carboxamide (SR141716; **5**) were synthesized to investigate the structure–activity relationship (SAR) of the aminopiperidine region. The structural modifications include the substitution of alkyl hydrazines, amines, and hydroxyalkylamines of varying lengths for the aminopiperidinyl moiety. Proximity and steric requirements at the aminopiperidine region were probed by the synthesis of analogues that substitute alkyl hydrazines of increasing chain length and branching. The corresponding amide analogues were compared to the hydrazides to determine the effect of the second nitrogen on receptor binding affinity. The *N*-cyclohexyl amide **14** represents a direct methine for nitrogen substitution for **5**, reducing the potential for heteroatom interaction, while the morpholino analogue **15** adds the potential for an additional heteroatom interaction. The series of hydroxyalkyl amides of increasing chain length was synthesized to investigate the existence of additional receptor hydrogen bonding sites. In displacement assays using the cannabinoid agonist [³H](1*R*,3*R*,4*R*)-3-[2-hydroxy-4-(1,1-dimethylheptyl)phenyl]-4-(3-hydroxypropyl) cyclohexan-1-ol (CP 55 940; **2**) or the antagonist [³H]**5**, **14** exhibited the highest CB₁ affinity. In general, increasing the length and bulk of the substituent was associated with increased receptor affinity and efficacy (as measured in a guanosine 5'-triphosphate- γ -[³⁵S] assay). However, in most instances, receptor affinity and efficacy increases were no longer observed after a certain chain length was reached. A quantitative SAR study was carried out to characterize the pharmacophoric requirements of the aminopiperidine region. This model indicates that ligands that exceed 3 Å in length would have reduced potency and affinity with respect to **5** and that substituents with a positive charge density in the aminopiperidine region would be predicted to possess increased pharmacological activity.

Introduction

The use of marijuana and cannabinoid preparations for medicinal purposes has been known for thousands of years; yet, its utility in recent years has been limited because of its psychoactive properties. The isolation and characterization of the primary psychoactive constituent of marijuana, Δ^9 -tetrahydrocannabinol (Δ^9 -THC; **1**), led to the study of the structure–activity relationships (SAR) of the cannabinoids.^{1,2} Ultimately, other cannabimimetic compounds were discovered, including compounds with structures differing quite dramatically from that of “classical” cannabinoid compounds, such as (1*R*,3*R*,4*R*)-3-[2-hydroxy-4-(1,1-dimethylheptyl)phenyl]-4-(3-hydroxypropyl) cyclohexan-1-ol (CP 55 940; **2**),³ the aminoalkylindole (*R*)-(+)-[2,3-dihydro-5-methyl-3-(morpholinyl)methyl]pyrrolo[1,2,3-*de*]-1,4-benzoxazinyl]- (1-naphthalenyl)methanone mesylate (WIN55 212-2; **3**),⁴ and the endogenous cannabinoid arachidonyl-

ethanolamide (anandamide; **4**)⁵ (Figure 1). These compounds led to the identification and characterization of cannabinoid receptors in the central nervous system (CB₁)^{6–8} and the periphery (CB₂).⁹

The discovery of *N*-(piperidinyl)-5-(4-chlorophenyl)-1-(2,4-dichlorophenyl)-4-methyl-1*H*-pyrazole-3-carboxamide (SR141716; **5**), a potent CB₁ receptor antagonist with nanomolar affinity,^{10,11} provides a unique chemical tool for further characterization of the cannabinoid pharmacophore in its relationship to the binding domain of cannabinoid antagonists. Alkyl hydrazides of increasing steric demand were synthesized to probe the volume of the aminopiperidine binding site. The amide analogues were compared to the hydrazides to assess the role of the second nitrogen. The *N*-cyclohexylamide analogue represented a direct methine for nitrogen substitution for **5**. The morpholino analogue added a further heteroatom interaction while the hydroxyalkyl amides of increasing chain length sought out a receptor hydrogen-bonding site. Finally, the (*R*)- and (*S*)-2-hydroxymethylethyl amides had an analogy to the (*R*)-

* To whom correspondence should be addressed. Tel.: (919)541-6552. Fax: (919)541-6499. E-mail: bft@rti.org.

[†] Research Triangle Institute.

[‡] University of Aberdeen.

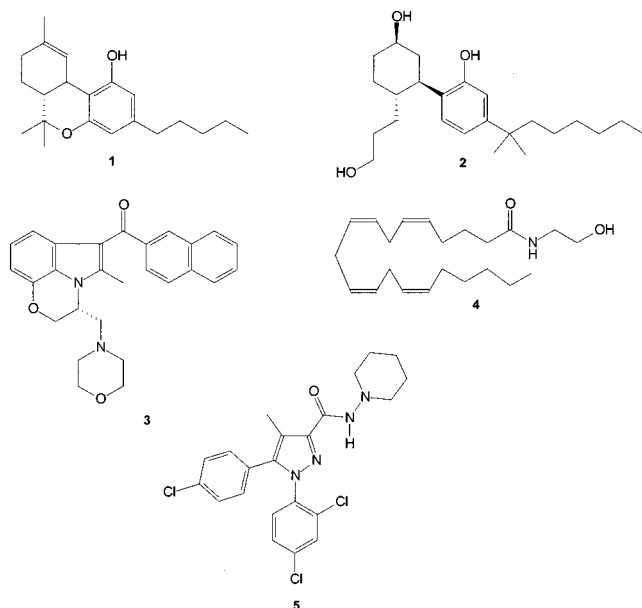


Figure 1. Examples of cannabinoid agonists and antagonists.

and (*S*)-methanandamides¹² and probed potential chirality requirements.

There is no direct knowledge of the atom-to-atom interactions between any cannabinoid ligand and the CB₁ or CB₂ cannabinoid receptors. Instead, pharmacophoric elements of each structural class's interaction with these receptors have been inferred using indirect approaches, such as receptor binding analyses of a variety of cannabinoid analogues using wild-type and mutated receptor systems^{13,14} and through the use of computer-aided molecular modeling techniques.^{15–23}

In the present study, quenched molecular dynamics were used to characterize the conformational space available to each analogue. These conformations were then included in quantitative SAR (QSAR) analyses and used to generate three-dimensional pharmacophore models. The models were derived using receptor binding affinity and efficacy measurements (guanosine 5'-triphosphate (GTP)- γ -[³⁵S]) as dependent variables. This approach builds on previous studies, which have utilized the multiplicity of conformers generated by molecular dynamics to determine and compare conformationally accessible regions in structure–activity analyses.^{21,24,25} The results of the study indicated that the pharma-

Scheme 1

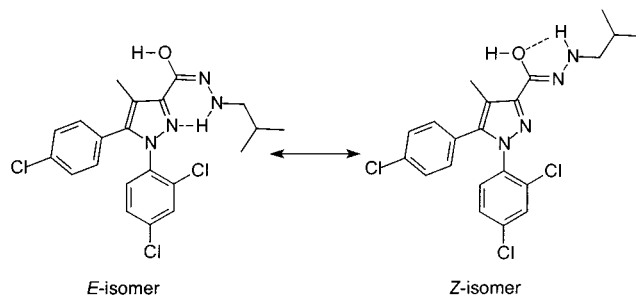
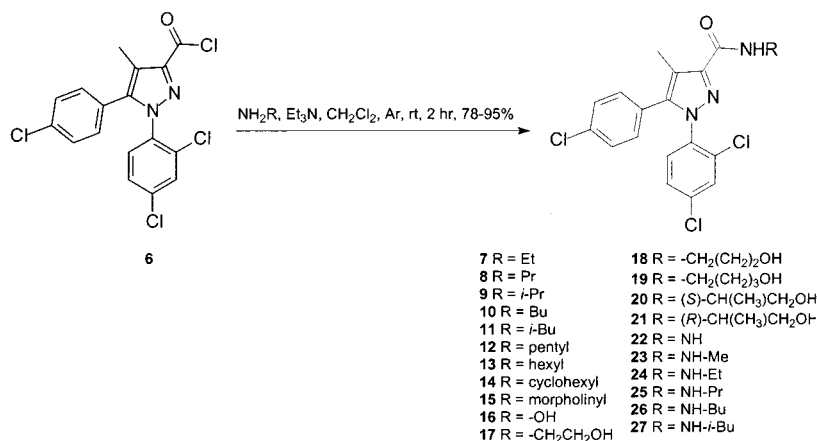


Figure 2. Postulated H bond-stabilized resonance isomers of **27**.

cophore models could fit the affinities and efficacies at the CB₁ receptor (with correlation coefficient greater than that derived for random target variables) but could not fit the affinities of these compounds at the CB₂ receptor. Thus, the results suggest that the SAR derived from these analogues can aid in the further design and synthesis of analogues and facilitate the elucidation of the cannabinoid pharmacophore for CB₁ selective antagonists.

Chemistry

The syntheses of the target compounds **7–21** were carried out in a manner similar to a previously published synthesis of **5**^{10,26–28} by condensation of the respective hydrazines and amines with the pyrazole acid chloride **6** and are shown in Scheme 1.

The various alkyl hydrazines (R = Et, Pr, Bu, *i*-Bu) were prepared by condensation of *tert*-butyl carbazate with the appropriate aldehydes,²⁹ followed by reduction with lithium aluminum hydride and subsequent acidic hydrolysis.³⁰ The syntheses of the alkyl hydrazide analogues **22–27** were then carried out as above (Scheme 1). The products were characterized by ¹H nuclear magnetic resonance (NMR), high resolution (electron impact (EI) and fast atom bombardment (FAB)) mass spectroscopy, high-performance liquid chromatography (HPLC), and analytical thin-layer chromatography (TLC).

The *N*-monoalkylhydrazides exhibited ¹H NMR evidence of a mixture of the H bond-stabilized *Z* and *E* tautomers shown in Figure 2. Using **27** as a representative example, two sets of peaks were observed for each of the hydrazide nitrogen, methylene, and methyl protons of the alkyl group at ambient temperature (295

K). Variable temperature ^1H NMR showed broadening of the above resonances with increasing temperature that led to coalescence into one set of peaks (δ 4.96, 3.51, and 0.85) at 329 K. After it was cooled to 295 K, the original spectrum was regenerated. This trend was noticeably absent from the amide, *N,N*-dialkylhydrazide (i.e., **5** and **15**), and hydroxyalkyl amide series, likely due to the lack of the H-bonding interactions postulated as a stabilizing influence. The tautomer distribution ratio was solvent-dependent, increasingly favoring one tautomer as solvent polarity decreased, MeOH- d_4 (1.9:1), DMSO- d_6 (2.0:1), pyridine- d_5 (2.4:1), and CDCl_3 (3.6:1).

The presence of an isomeric mixture with significant stability of two forms has potential ramifications for the structure–activity interpretation of SR analogues since the two isomers are likely to have different affinity and efficacy profiles at the receptor. The rotamer of the potent archetype compound **5** that is observed in the crystal form is the *Z* isomer. Because this is generally regarded as the ground state conformation of the molecule, the corresponding *Z* tautomers of the *N*-monoalkylhydrazides (**23**–**27**) can be viewed as the active conformation corresponding to **5**. The design of future analogues that reside preferentially in the putative active *Z* conformation would be anticipated to be the more active structures. Designing for conformational preference would, at least, test this concept.

Molecular Modeling. Molecules and QSAR analyses were performed using SYBYL (Tripos Inc., St. Louis, MO). Electrostatic charges of each compound were calculated with the Gasteiger–Hückel method. Each compound was energy-minimized using the SYBYL force field with a conjugate gradient of 0.001 kcal/mol or a maximum of 100 000 iterations as termination criteria.

Quenched Molecular Dynamics. Molecular dynamics were computed on each energy-minimized structure at temperatures from 100 to 1000 K. At each 100 K step, the molecule was allowed to remain at the specified temperature for 1 ps while snapshots of the conformation were acquired every 1 ps. After the temperature reached 1000 K, the molecule was held at this temperature for 1 ps while snapshots were acquired at 1 ps intervals. This procedure yielded a total of 100 snapshots of different conformers for each molecule investigated. Gasteiger–Hückel charges were taken into consideration throughout this molecular dynamics procedure. Each conformation obtained for a particular molecule was then energy-minimized again using a conjugate gradient of 0.01 kcal/mol or a maximum of 100 000 iterations as termination criteria, yielding a group of 100 energy-minimized conformers per compound.

Molecular and Conformational Alignment. One conformation of one compound was used as a template molecule; it was unimportant which molecule was used for this template so long as it was applied consistently, because the pyrazole ring systems of all analogues were identical. All conformations of all compounds were aligned in space so as to overlay as closely as possible the five atoms of their pyrazole ring system with the corresponding atoms in the template molecule. The alignment was performed using atom-by-atom root

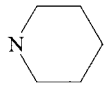
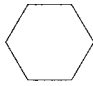
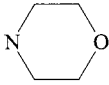
mean square distance minimization. This alignment positions all of the molecules in the same three-dimensional space and superimposes the ring systems to as great an extent as possible. Because the alkyl amide and alkyl hydrazide side chains are not part of the alignment rule, this feature of the molecule could be compared between conformers of the same compound as well as between different compounds using the QSAR techniques described below.

Quantitative Structure–Activity Analyses. The biological data used as the target values for the structure–activity analyses included CB_1 and CB_2 receptor binding affinity and efficacy in a GTP- γ - ^{35}S assay. Comparative molecular field analysis (CoMFA) was used for the QSAR and involved all of the compounds shown in Table 1. In this approach, the descriptive variables are steric and electrostatic descriptions of the three-dimensional structures of the entire set of compounds. This technique has been previously used successfully in QSAR studies of cannabinoids.^{20,22,25,31,32} The CoMFA analysis was performed using a proton (H^+) probe atom positioned at lattice points spaced around the molecules at 2 Å increments. With cross-validation groups set to 5, a cross-validation study was carried out by randomly selecting 80% of the compounds to form a training set, developing a QSAR model based on their three-dimensional steric and electrostatic properties, and using this model to predict the dependent variables of the remaining 20% of the compounds that were not included in the training set. The predicted dependent variable of the compounds that was omitted from the training set was then compared against the actual dependent variable (e.g., receptor affinity), and a correlation coefficient was obtained. This process was repeated randomly until every compound had been omitted from the training set and had its dependent variables predicted at least once. The correlation coefficients of the entire process were tracked throughout this process, and the average r^2 value was calculated as a measure of the press or the goodness/robustness of the model. Cross-validation studies were also conducted using a “leave-one-out” strategy where the model was derived repetitively, each new run excluding one particular compound from the training set. This was repeated so that each compound was excluded from the training set and its affinity/potency predicted by a model derived on the remaining compounds. For each compound, 50 random conformers were selected for each QSAR analysis. Control studies were also run where randomized pharmacological data were used in place of real pharmacological data. These artificial points were random numbers generated to fall within the range of the real data. The same cross-validated and final analyses were performed in the control studies to check that the r^2 values were higher when pharmacological data were used than when artificial data were used.

Results and Discussion

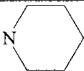

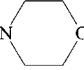
Receptor Binding Studies. CB_1 Receptor Affinities. The binding affinities of each compound as measured in competition assays (K_i values) with [^3H]**2** and [^3H]**5** in rat whole brain membrane preparations are provided in Table 1. The K_i of **5** is reported as a reference. These data demonstrate that as the size of

Table 1. Radioligand Binding Data for Amide and Hydrazone Analogues of 5

R	Compound	Whole Brain K_i (nM \pm SEM ^a)		CB ₂ K_i	CB ₁	[³⁵ S]GTP- γ -S	
		[³ H]2	[³ H]5	(nM \pm SEM ^a)	Selectivity (CB ₂ /CB ₁)	EC ₅₀ (nM \pm SEM)	E _{max}
	5	6.18 \pm 1.20	1.18 \pm 0.10	313 ^b	51	56300 \pm 14300	-37.8
CH ₂ CH ₃	7	46.3 \pm 1.5	61.5 \pm 3.3	3110 \pm 610	67	30300 \pm 5000	-46.9
CH ₂ CH ₂ CH ₃	8	29.9 \pm 0.6	23.6 \pm 1.1	2960 \pm 2100	99	11100 \pm 3700	-35.7
CH(CH ₃) ₂	9	29.4 \pm 0.8	12.9 \pm 4.7	1740 \pm 580	59	16000 \pm 4700	-46.4
CH ₂ (CH ₂) ₂ CH ₃	10	13.4 \pm 1.0	12.8 \pm 1.6	1600 \pm 430	119	8540 \pm 3100	-38.5
CH ₂ CH(CH ₃) ₂	11	11.5 \pm 0.2	9.22 \pm 0.17	704 \pm 130	61	7540 \pm 10	-11.0
CH ₂ (CH ₂) ₃ CH ₃	12	11.4 \pm 0.5	6.83 \pm 1.20	1110 \pm 240	97	5270 \pm 1700	-7.4
CH ₂ (CH ₂) ₄ CH ₃	13	18.1 \pm 4.0 ^c	10.7 \pm 0.6	6870 ^b	378	29400 \pm 16100	-13.0
	14	2.46 \pm 0.10	1.07 \pm 0.13	228 \pm 2	93	26000 ^b	-22.1
	15	22.9 \pm 2.2	21.0 \pm 2.2	2400 \pm 780	105	38900 \pm 28400	-76.3
OH	16	1690 \pm 480	1560 \pm 630	7820 ^b	5	not tested	-
CH ₂ CH ₂ OH	17	385 \pm 13	343 \pm 8	4270 \pm 570	11	1670000 ^d \pm 658000	-76.5
CH ₂ (CH ₂) ₂ OH	18	160 \pm 19	156 \pm 3	1250 \pm 280	8	241000 \pm 39200	-83.3
CH ₂ (CH ₂) ₃ OH	19	154 \pm 2	143 \pm 12	5720 ^b	37	304000 \pm 131000	-79.5
(S)-(+) CH(CH ₃)CH ₂ OH	20	117 \pm 0	123 \pm 2	5900 \pm 2800	50	294000 \pm 11700	-83.8
(R)-(-) CH(CH ₃)CH ₂ OH	21	117 \pm 28	99.8 \pm 3.9	1770 \pm 140	15	292000 \pm 43500	-83.0
NH ₂	22	374 \pm 27	602 \pm 58	12100 \pm 170	32	419000 ^d \pm 53200	-71.7
NHCH ₃	23	555 \pm 86	429 \pm 46	6660 \pm 930	12	12000000 ^b	-63.8
NHCH ₂ CH ₃	24	143 \pm 9	72.0 \pm 7.6	6061 \pm 900	42	495000 ^d \pm 162000	-81.4
NH(CH ₂) ₂ CH ₃	25	74.8 \pm 11.5	64.0 \pm 12.1	2620 \pm 440	35	105000 \pm 17500	-85.0
NH(CH ₂) ₃ CH ₃	26	50.9 \pm 6.4	40.6 \pm 1.5	2850 \pm 160	56	128000 \pm 18900	-72.7
NHCHCH(CH ₃) ₂	27	41.8 \pm 1.6	35.5 \pm 1.2	2190 \pm 760	52	73600 \pm 20300	-78.1

^a $n = 2$ unless otherwise noted. ^b $n = 1$. ^c $n = 6$. ^d Value greater than highest point on displacement curve.

Table 2. Receptor Antagonism in Mouse Vas Deferens

R	Compound	Compound Concentration (nM) ^a	K _B (nM) (95% confidence limits)
	5	31.6	0.4 (0.2, 0.8)
	14	31.6	1.2 (0.3, 3.8)
	15	316	12.5 (6.8, 23.9)
CH ₂ (CH ₂) ₄ CH ₃	13	31.6	15.4 (5.4, 91.2)
CH ₂ CH(CH ₃) ₂	11	316	21.2 (10.8, 49.7)
CH ₂ (CH ₂) ₃ CH ₃	12	316	31.7 (14.1, 74.2)

^a Concentration of compound used to determine the dissociation constant, K_B, which was determined in the mouse-isolated vas deferens using the cannabinoid receptor agonist **3**.

the carbon chain is increased, modest increases in the binding affinity are observed, up to the C-5 chain. With the C-6 chain, increases in binding affinity are no longer evident. This trend is apparent in the alkyl amides **7–13**, the hydroxyalkyl amides **16–21**, and the alkyl hydrazides **22–27**. The presence of a chiral center in the compound appeared not to be a factor as there was not a significant difference in the binding affinity to the receptor between the (*R*)- and (*S*)-hydroxymethylethyl amides (**20** and **21**). They both exhibited a 20-fold decrease in binding affinity over **5**, as did the rest of the hydroxyalkyl amide series. This implies that the presence of the second electronegative heteroatom decreases the receptor binding affinity.

When a methylene unit in the piperidinyl ring is replaced with an oxygen, as in the morpholino derivative **15**, only moderate binding affinity is observed, again implying that the electronegativity of the oxygen decreases receptor binding affinity. Similarly, the replacement of the nitrogen atom in the piperidinyl ring of **5** with a methylene group (**14**) results in modest increases in CB₁ affinity (when measured with [³H]**2**) and efficacy (discussed later). This suggests that the piperidinyl ring nitrogen is not likely involved in electrostatic interactions or hydrogen bond formation with the receptor that promotes higher affinity/efficacy.

CB₂ Receptor Affinities. Most of the structural modifications did not appear to have much effect on CB₁/CB₂ selectivity, primarily because none of the compounds tested were found to possess high affinity for the CB₂ receptor. The majority of those compounds showing a modest increase in selectivity for the CB₁ receptor over that of **5** were in the alkyl amide and cyclic analogues. Typically, the affinities of the hydrazide analogues for the CB₂ receptors were even lower than that of **5**, but their CB₁ affinity was even more dramatically reduced. Thus, in this set of compounds, both affinity and selectivity for the CB₁ receptor were decreased.

GTP-γ-[³⁵S] Binding Assay. The GTP-γ-[³⁵S] assays were conducted according to a variation of Sim et al.³³

In general, EC₅₀ values in this test system paralleled observed trends in CB₁ receptor affinity. For example, the EC₅₀ values of the alkyl amides decreased as the carbon chain increased from ethyl to pentyl but then increased again with the hexyl analogue. In all instances, these compounds behaved as inverse agonists. The E_{max} values in the alkyl amides were similar to that observed with **5** up until a straight chain length of four was reached, after which the E_{max} values were lower. In one compound (**12**), the inverse agonist activity was only -7.4% of control, indicating that this compound was a very weak inverse agonist in this system.

In Vitro Pharmacology: Mouse Vas Deferens Assay. It has been established that cannabinoid agonists, such as **3**, can inhibit electrically evoked contractions of isolated tissue preparations such as the mouse vas deferens.³⁴ Five compounds with reasonably high affinity for the CB₁ receptor were tested for their ability to antagonize this effect (Table 2). In all of these experiments, a dose-response curve to **3** was constructed 30 min after administration of either the test compound, compound **5**, or vehicle (*n* = 5 or 6). All five of the compounds produced parallel dextral shifts in the dose-response curve of **3**, with **14** being the most potent of the compounds tested. Compounds **12**, **14**, and **15** also exhibited a significant inverse effect (enhancement of twitch amplitude immediately before the first addition of **3**). Compounds **11** and **13** did not exhibit this inverse effect at the concentrations tested.

Molecular Modeling and QSAR Analyses. Quenched Molecular Dynamics. The quenched molecular dynamics approach used for conformational sampling generated 100 low-energy conformations for each molecule. The conformations were quite diverse for certain molecules, while other molecules repeatedly yielded a small number of similar conformations. These differences in conformational mobility can be visualized graphically by overlaying the conformations for a particular molecule (Figure 3). Visual inspection of the conformational ensembles for this series of analogues

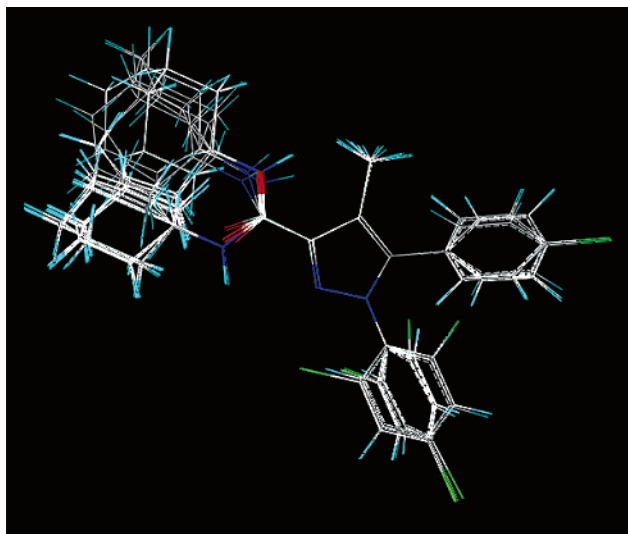


Figure 3. Graphical representation of the conformational ensemble obtained by quenched molecular dynamics for **14**.

of **5** suggests that a full and representative sample of conformations was afforded by this technique.

CoMFA. The CoMFA approach is typically applied to single conformations selected for each analogue and usually involves the identification of a bioactive conformer or the selection of a putative bioactive conformation. The data and results achieved during these QSAR studies are dependent on the molecular alignment system used to compare analogues. We chose to align molecules by overlaying their pyrazole rings using a root mean square minimization procedure, thereby maximizing the structural differences of the training set in the aminopiperidinyl region. This alignment strategy is arguably the most appropriate, because the two-dimensional structure of the compounds differed only in the aminopiperidinyl region. Furthermore, the three-dimensional conformational mobility of these analogues also differed primarily in the aminopiperidinyl region.

Regardless of the number of conformations used for each analogue or sampling strategy, the cross-validated analysis of the relationship between the CoMFA molecular fields and the pharmacological affinity and potency measurements generally indicated that a model derived with (the maximum of) five components was optimal. Components are the variables used by SYBYL in developing the QSAR model; five components indicate that five parameters were varied to achieve the predicted data used in the "predicted vs actual" linear regression fit. Note that components do not have a specific physical analogue: they are neither regions of the molecule nor pharmacological assays but simply a facet of the numerical techniques used to develop a QSAR model. The larger number of components in an equation created to explain activity indicates a more complex and less robust model.

The strength of the cross-validated and final models was demonstrated by comparison with relationships derived with random pharmacological data that spanned the same range as the real pharmacological data, and this is illustrated in Figure 4. This CoMFA analysis utilized 50 conformations of each of the 21 molecules listed in Table 1 (1050 conformers total) in the training set. Cross-validated r^2 values of 0.675, 0.691, 0.402, and

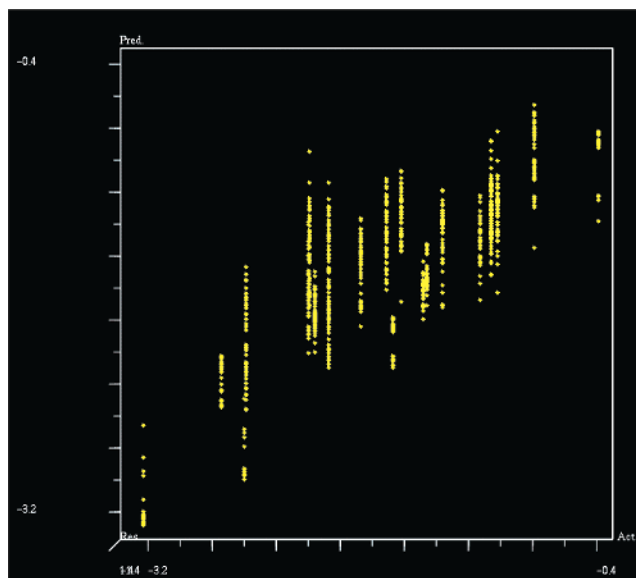


Figure 4. Potency of analogues of **5** as predicted by QSAR model.

Table 3. QSAR Model Derived with Real or Random Data

dependent variable	r^2 values			
	real data		random data	
	cross	final	cross	final
pK_i , CB ₁ (³ H) 2)	0.675	0.701	0.145	0.263
pK_i , CB ₁ (³ H) 5)	0.691	0.717	0.128	0.224
pK_i , CB ₂ (³ H) 2)	0.402	0.464	0.054	0.213
pK_{EC50} (GTP- γ - ³⁵ S))	0.168	0.276	0.310	0.365

0.168 were obtained for the CB₁ receptor affinities utilizing [³H]**2** and [³H]**5**, CB₂ receptor affinity, and efficacy in a GTP- γ -³⁵S] assay, respectively. When random pharmacological data were used, values of 0.145, 0.128, 0.054, and 0.310 were obtained for the CB₁ receptor affinities utilizing [³H]**2** and [³H]**5**, CB₂ receptor affinity, and efficacy in a GTP- γ -³⁵S] assay, respectively. The final analysis (based on all 1050 conformers being included in the training set) resulted in r^2 values of 0.701, 0.717, 0.464, and 0.276 with real data and 0.263, 0.224, 0.213, and 0.365 for random data (in models derived for CB₁ receptor affinities utilizing [³H]**2** and [³H]**5**, CB₂ receptor affinity, and efficacy in a GTP- γ -³⁵S] assay, respectively). The results, which are listed in Table 3, indicated that pharmacophore models could fit the affinities of these compounds at the CB₁ receptor but could not fit the affinities of these compounds at the CB₂ receptor nor their efficacies in a GTP- γ -³⁵S] assay.

Visualization of CoMFA Fields. Three-dimensional contour plots of the CoMFA model allow the visualization of regions where changes in steric or electrostatic properties are correlated with experimentally determined differences in biological properties. The contour plots in Figures 5 and 6 display the QSAR model for receptor affinity in the CB₁ receptor assay utilizing [³H]-**2** as radioligand when derived from a training set of 1050 conformers (50 random conformations from each of 21 molecules). Some of the most heavily weighted regions in the model are depicted in the contour plot at the 80/20 level.

Inspection of the steric contour plot (Figure 5) reveals that the aminopiperidinyl region of **5** was surrounded

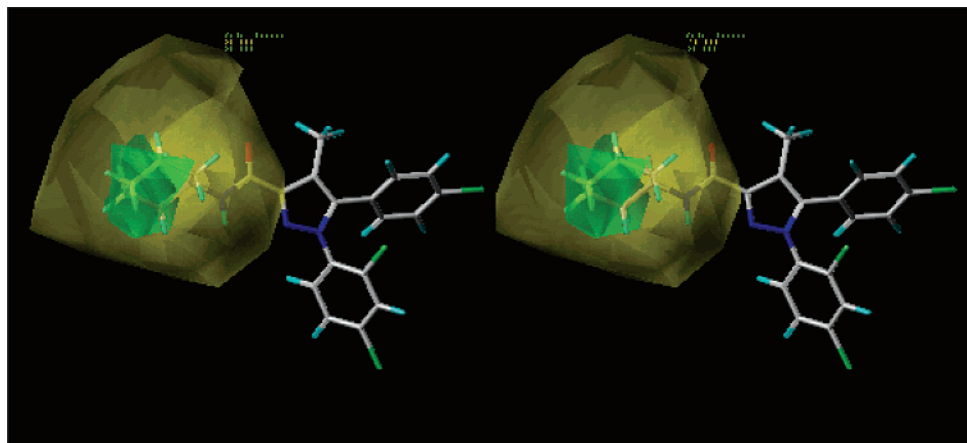


Figure 5. Stereoview of the QSAR derived for the steric fields (yellow and green contours) for CB₁ binding affinity utilizing [³H]2 as radioligand. The steric plot is depicted so that steric bulk should be moved closer to areas contoured in green and farther from regions contoured in yellow in order to increase the predicted target property (i.e., affinity). For this model, an 80/20 level of contribution is depicted; 80 indicates that the region displayed is that which contributes within the top 20% of the (green) interaction, and 20 indicates that the region displayed is that which contributes within the top 20% of negative (yellow) interactions.

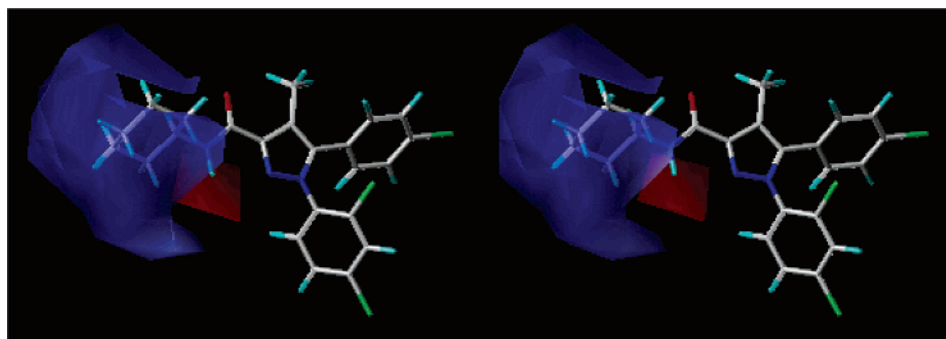


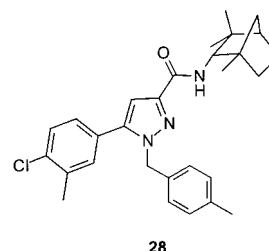
Figure 6. Stereoview of the QSAR derived for the electrostatic field (blue and red contours) for CB₁ binding affinity utilizing [³H]2 as radioligand. The electrostatic plot is contoured such that the positive charge should be moved closer to regions contoured in blue and farther from regions contoured in red in order to increase the target property being contoured.

by a green contour, indicating a region where steric bulk is associated with increased predicted pharmacological potency. Ligands substituted at the aminopiperidinyl region of **5** that exceed 3 Å in length are predicted to have reduced potency and affinity with respect to **5**. This predicted decrease in potency and affinity corresponds to the amide and hydrazide analogues exceeding five carbons in length.

Examination of the electrostatic plot in Figure 6 reveals a large contour in blue that completely surrounds the aminopiperidinyl region and a smaller red contour that covers only the amide linkage. The blue contour indicates that compounds with positive charge densities in this region would be predicted to possess increased pharmacological activity while the regions contoured in red are indicative of where negative charge is associated with increased pharmacological activity. Therefore, one could suggest that in the hydroxyalkyl amides, the presence of the electronegative oxygen atom in the blue-contoured region leads to their decreased affinity, resulting in compounds with *K_i* values ranging from 117 to 1686 nM.

The results of the study demonstrate that three-dimensional pharmacophore models derived for a variety of analogues of **5** can fit their affinities and efficacies at the CB₁ receptor (with a correlation coefficient greater than that derived for random target variables) but cannot fit the affinities of these compounds at the CB₂ receptor. This is consistent with the observation

that the CB₂ selective antagonist *N*-[(1*S*)-endo-1,3,3-trimethylbicyclo[2.2.1]heptan-2-yl]-5-(4-chloro-3-methylphenyl)-1-(4-methylbenzyl)-1*H*-pyrazole-3-carboxamide (SR144528; **28**) has structural modifications in addition to the change at the aminopiperidine moiety (replaced by the (1*S*)-endo-fenchylamine group in **28**) that was explored. These changes, which include replacement of the phenyl group on nitrogen 1 with a substituted benzyl group and the elimination of the methyl group on the pyrazole ring, could be more responsible for the complete inversion of the CB₁/CB₂ selectivity of **28** as compared to **5**. Indeed, one might suggest that these regions need to be included in QSAR studies involving CB₂ affinity, thereby illustrating how the SAR derived from these analogues can aid in the further design and synthesis of analogues of **5**.



28

Conclusions

On the basis of the results reported here, as the length of the carbon chain increases, the affinity of the ana-

logues of **5** increases but only up to the C-5 chain. When the chain is six carbons long, gains in affinity toward the CB₁ receptor are no longer observed. This trend is consistent over the alkyl hydrazide, the alkyl amide, and the hydroxyalkyl amide series. When comparing the receptor binding affinities of **5** and **14**, it is apparent that the nitrogen atom in the piperidiny moiety is not contributing to the affinity of **5**. In addition, the binding affinity for the alkyl hydrazide series decreased relative to **5**, which lends support to the theory that the second nitrogen atom as a 2° nitrogen is not contributing to the overall binding affinity. The presence of the second heteroatom in the case of the morpholino amide **15** and the hydroxyalkyl amide series **16–21** also decreased the receptor binding affinity.

From the SAR studies, consistent data have been acquired, which indicates that the pharmacophoric requirements of the aminopiperidine region involve having a side chain no greater than 3 Å in length. In addition, having a substituent with a positive charge density in the aminopiperidine region is predicted to result in compounds with increased affinity and potency toward the CB₁ receptor. The consistent applications of the methods and the comparison of these results with the randomized data lend support for these pharmacophoric requirements of the aminopiperidine region.

Experimental Section

General Methods. Reactions were conducted under N₂ or Ar atmospheres using oven-dried glassware. All solvents and chemicals used were reagent grade. Tetrahydrofuran (THF) and Et₂O were distilled from sodium benzophenone ketyl under N₂. CH₂Cl₂, hexanes, and toluene were passed through basic alumina and stored over 4 Å molecular sieves under Ar. Et₃N was distilled from CaH₂ and stored over NaOH pellets under Ar. Unless otherwise mentioned, reagents were obtained from commercial sources and used without further purification. Melting points were determined on a Mel-Temp apparatus and are uncorrected. The optical rotations were determined on a Rudolph Autopol III spectropolarimeter. Flash column chromatography was carried out with Whatman silica gel 60 (230–400 mesh). Purity and characterization of compounds were established by a combination of HPLC, TLC, gas chromatography mass spectrometry (GC-MS), high-resolution mass spectrometry (HRMS), and NMR analytical techniques described below. Compounds were shown to be homogeneous by HPLC employing two diverse solvent mixtures on a Waters dual pump chromatograph operating at 2.0 mL/min with a model 484 tunable absorbance detector, Waters Nova-Pak reversed phase C-18 (4 μm) RCM 8 mm × 100 mm column, UV detection at 280 nm; eluents utilized were either CH₃CN–H₂O or CH₃OH–H₂O mixtures as indicated in each experimental procedure. TLC on Whatman Si254F silica gel glass plates eluting with the solvents indicated in each experimental procedure, and employing UV and phosphomolybdic acid–ceric sulfate spray and/or iodine detection, similarly showed the homogeneity of the compounds. GC-MS was measured on a Hewlett-Packard 6890 GC System with a model 5973 Mass Selective Detector using EI ionization. HRMS were determined on a VG-70S Mass Spectrometer (Micromass; Beverly, MA) and were performed by the mass spectrometry laboratory at the University of South Carolina. ¹H NMR spectra were recorded on a Bruker Avance DPX-300 (300 MHz) spectrometer and were determined in MeOH-*d*₄ with tetramethylsilane (TMS) (0.00 ppm) or MeOH (3.30 ppm) as the internal reference unless otherwise noted. Variable temperature ¹H NMR spectra were recorded on a Bruker AMX-500 (500 MHz) and were determined in DMSO-*d*₆ with TMS (0.00 ppm) as the internal reference. Temperatures were uncorrected. For tautomeric mixtures (**25–27**), fractional proton resonances were reported as observed.

N-Ethyl-5-(4-chlorophenyl)-1-(2,4-dichlorophenyl)-4-methyl-1H-pyrazole-3-carboxamide (7). Ethylamine (2.0 M solution in THF, 0.5 mL, 1.00 mmol), triethylamine (280 μL, 2.00 mmol), and CH₂Cl₂ (5 mL) were cooled to 0 °C under argon and treated dropwise over 5 min with a solution of **6**^{27,28} (218.6 mg, 0.55 mmol) in CH₂Cl₂ (5 mL). The solution was allowed to warm slowly to 25 °C under Ar and stirred for an additional 2 h. The reaction was quenched by addition of 10 mL of H₂O and partitioned. The organic layer was washed with 2 × 20 mL of 1 N HCl. The combined aqueous layers were back-extracted with CH₂Cl₂, and the combined CH₂Cl₂ layers were washed with saturated aqueous NaHCO₃. The aqueous layer was back-extracted with CH₂Cl₂, and the combined CH₂Cl₂ layers were dried over Na₂SO₄. The CH₂Cl₂ was evaporated in vacuo, yielding a brown foam. Flash chromatography (1:1 EtOAc–hexanes) yielded the product as a white foam (200 mg, 90% yield); mp 119.2–119.8 °C. ¹H NMR: δ 7.57 (d, *J* = 2.2 Hz, 1H, Ar 3-H), 7.52 (d, *J* = 8.5 Hz, 1H, Ar 6-H), 7.44 (dd, *J* = 2.2, 8.5 Hz, 1H, Ar 5-H), 7.36 (d, *J* = 8.5 Hz, 2H, Ar' 3,5-H), 7.19 (d, *J* = 8.5 Hz, 2H, Ar' 2,6-H), 3.39 (q, *J* = 7.2 Hz, 2H, N–CH₂–CH₃), 2.30 (s, 3H, CH₃), 1.21 (t, *J* = 7.2 Hz, 3H, N–CH₂–CH₃). HPLC: 65% CH₃CN–H₂O, *R*_t 10.4 min (100%); 85% CH₃OH–H₂O, *R*_t 4.3 min (100%). TLC: 4:1 EtOAc–Hex, *R*_f 0.68; 10% MeOH–CHCl₃, *R*_f 0.70. HREIMS: *m/z* 407.0360 (calcd for C₁₉H₁₆³⁵Cl₃N₃O, 407.0359).

N-(1-Propyl)-5-(4-chlorophenyl)-1-(2,4-dichlorophenyl)-4-methyl-1H-pyrazole-3-carboxamide (8). Compound **8** was obtained from **6** and 1-propylamine according to the procedure described for **7** and was isolated as a white semisolid (208 mg, 88% yield). ¹H NMR: δ 7.57 (d, *J* = 2.2 Hz, 1H, Ar 3-H), 7.53 (d, *J* = 8.5 Hz, 1H, Ar 6-H), 7.44 (dd, *J* = 2.2, 8.5 Hz, 1H, Ar 5-H), 7.36 (d, *J* = 8.5 Hz, 2H, Ar' 3,5-H), 7.19 (d, *J* = 8.6 Hz, 2H, Ar' 2,6-H), 3.35 (t, *J* = 7.7 Hz, 2H, N–CH₂–CH₂–CH₃), 2.30 (s, 3H, CH₃), 1.64 (m, 2H, N–CH₂–CH₂–CH₃), 0.97 (t, *J* = 7.4 Hz, 3H, N–CH₂–CH₂–CH₃). HPLC: 65% CH₃CN–H₂O, *R*_t 14.9 min (100%); 85% CH₃OH–H₂O, *R*_t 4.8 min (100%). TLC: 4:1 EtOAc–Hex, *R*_f 0.72; 10% MeOH–CHCl₃, *R*_f 0.73. HREIMS: *m/z* 421.0519 (calcd for C₂₀H₁₈³⁵Cl₃N₃O, 421.0515).

N-(2-Propyl)-5-(4-chlorophenyl)-1-(2,4-dichlorophenyl)-4-methyl-1H-pyrazole-3-carboxamide (9). Compound **9** was obtained from **6** and 2-propylamine according to the procedure described for **7** and was isolated as a white semisolid (207 mg, 95% yield). ¹H NMR: δ 7.57 (d, *J* = 2.2 Hz, 1H, Ar 3-H), 7.54 (d, *J* = 8.5 Hz, 1H, Ar 6-H), 7.45 (dd, *J* = 2.2, 8.4 Hz, 1H, Ar 5-H), 7.37 (d, *J* = 8.5 Hz, 2H, Ar' 3,5-H), 7.19 (d, *J* = 8.5 Hz, 2H, Ar' 2,6-H), 4.20 (hept, *J* = 6.6 Hz, 1H, N–CH(CH₃)₂), 2.30 (s, 3H, CH₃), 1.24 (d, *J* = 6.6 Hz, 6H, N–CH(CH₃)₂). HPLC: 65% CH₃CN–H₂O, *R*_t 14.5 min (100%); 85% CH₃OH–H₂O, *R*_t 5.1 min (100%). TLC: 4:1 EtOAc–Hex, *R*_f 0.73; 10% MeOH–CHCl₃, *R*_f 0.73. HREIMS: *m/z* 421.0502 (calcd for C₂₀H₁₈³⁵Cl₃N₃O, 421.0515).

N-(1-Butyl)-5-(4-chlorophenyl)-1-(2,4-dichlorophenyl)-4-methyl-1H-pyrazole-3-carboxamide (10). Compound **10** was obtained from **6** and 1-butylamine according to the procedure described for **7** and was isolated as a white semisolid (185 mg, 84% yield). ¹H NMR: δ 7.57 (d, *J* = 2.2 Hz, 1H, Ar 3-H), 7.53 (d, *J* = 8.5 Hz, 1H, Ar 6-H), 7.45 (dd, *J* = 2.2, 8.5 Hz, 1H, Ar 5-H), 7.37 (d, *J* = 8.5 Hz, 2H, Ar' 3,5-H), 7.19 (d, *J* = 8.5 Hz, 2H, Ar' 2,6-H), 3.36 (t, *J* = 7.1 Hz, 2H, N–CH₂–CH₂–CH₂–CH₃), 2.30 (s, 3H, CH₃), 1.59 (m, 2H, N–CH₂–CH₂–CH₂–CH₃), 1.41 (m, 2H, N–CH₂–CH₂–CH₂–CH₃), 0.96 (t, *J* = 7.3 Hz, 3H, N–CH₂–CH₂–CH₂–CH₃). HPLC: 65% CH₃CN–H₂O, *R*_t 20.5 min (100%); 85% CH₃OH–H₂O, *R*_t 5.7 min (100%). TLC: 4:1 EtOAc–Hex, *R*_f 0.75; 10% MeOH–CHCl₃, *R*_f 0.77. HREIMS: *m/z* 435.0679 (calcd for C₂₁H₂₀³⁵Cl₃N₃O, 435.0672).

N-(2-Methylpropyl)-5-(4-chlorophenyl)-1-(2,4-dichlorophenyl)-4-methyl-1H-pyrazole-3-carboxamide (11). Compound **11** was obtained from **6** and 2-methylpropylamine according to the procedure described for **7** and was isolated as a white semisolid (196 mg, 89% yield). ¹H NMR: δ 7.57 (d, *J* = 2.2 Hz, 1H, Ar 3-H), 7.53 (d, *J* = 8.5 Hz, 1H, Ar 6-H), 7.44 (dd, *J* = 2.2, 8.5 Hz, 1H, Ar 5-H), 7.36 (d, *J* = 8.5 Hz, 2H, Ar'

3,5-H), 7.19 (d, $J = 8.5$ Hz, 2H, Ar' 2,6-H), 3.18 (d, $J = 7.0$ Hz, 2H, N-CH₂-CH-(CH₃)₂), 2.30 (s, 3H, CH₃), 1.89 (m, 1H, N-CH₂-CH-(CH₃)₂), 0.96 (d, $J = 6.7$ Hz, 6H, N-CH₂-CH-(CH₃)₂). HPLC: 65% CH₃CN-H₂O, R_t 13.4 min (100%); 85% CH₃OH-H₂O, R_t 6.2 min (100%). TLC: 4:1 EtOAc-Hex, R_f 0.77; 10% MeOH-CHCl₃, R_f 0.72. HREIMS: m/z 435.0675 (calcd for C₂₁H₂₀³⁵Cl₃N₃O, 435.0672).

N-(1-Pentyl)-5-(4-chlorophenyl)-1-(2,4-dichlorophenyl)-4-methyl-1H-pyrazole-3-carboxamide (12). Compound **12** was obtained from **6** and 1-pentylamine according to the procedure described for **7** and was isolated as a colorless oil (206 mg, 88% yield). ¹H NMR: δ 7.61 (d, $J = 2.2$ Hz, 1H, Ar 3-H), 7.56 (d, $J = 8.4$ Hz, 1H, Ar 6-H), 7.48 (dd, $J = 2.2, 8.4$ Hz, 1H, Ar 5-H), 7.40 (d, $J = 8.5$ Hz, 2H, Ar' 3,5-H), 7.23 (d, $J = 8.5$ Hz, 2H, Ar' 2,6-H), 3.39 (t, $J = 7.2$ Hz, 2H, N-CH₂-(CH₂)₃-CH₃), 2.34 (s, 3H, CH₃), 1.65 (m, 2H, N-CH₂-CH₂-(CH₂)₂-CH₃), 1.40 (m, 4H, N-CH₂-CH₂-(CH₂)₂-CH₃), 0.96 (t, $J = 6.8$ Hz, 3H, N-(CH₂)₄-CH₃). HPLC: 65% CH₃CN-H₂O, R_t 19.3 min (100%); 85% CH₃OH-H₂O, R_t 6.4 min (100%). TLC: 4:1 EtOAc-Hex, R_f 0.81; 10% MeOH-CHCl₃, R_f 0.81. HREIMS: m/z 449.0838 (calcd for C₂₂H₂₂³⁵Cl₃N₃O, 449.0828).

N-(1-Hexyl)-5-(4-chlorophenyl)-1-(2,4-dichlorophenyl)-4-methyl-1H-pyrazole-3-carboxamide (13). Compound **13** was obtained from **6** and 1-hexylamine according to the procedure described for **7** and was isolated as a colorless oil (111 mg, 60% yield). ¹H NMR: δ 7.59 (d, $J = 2.2$ Hz, 1H, Ar 3-H), 7.54 (d, $J = 8.5$ Hz, 1H, Ar 6-H), 7.46 (dd, $J = 2.2, 8.5$ Hz, 1H, Ar 5-H), 7.38 (d, $J = 8.6$ Hz, 2H, Ar' 3,5-H), 7.21 (d, $J = 8.6$ Hz, 2H, Ar' 2,6-H), 3.39 (t, $J = 7.1$ Hz, 2H, N-CH₂-(CH₂)₄-CH₃), 2.32 (s, 3H, CH₃), 1.62 (m, 2H, N-CH₂-CH₂-(CH₂)₃-CH₃), 1.37 (m, 6H, N-CH₂-CH₂-(CH₂)₃-CH₃), 0.93 (t, $J = 6.8$ Hz, 3H, N-(CH₂)₅-CH₃). HPLC: 75% CH₃CN-H₂O, R_t 17.3 min (100%); 82% CH₃OH-H₂O, R_t 15.8 min (100%). TLC: 4:1 EtOAc-Hex, R_f 0.79; 10% MeOH-CHCl₃, R_f 0.82. HREIMS: m/z 463.0984 (calcd for C₂₃H₂₄³⁵Cl₃N₃O, 463.0985).

N-Cyclohexyl-5-(4-chlorophenyl)-1-(2,4-dichlorophenyl)-4-methyl-1H-pyrazole-3-carboxamide (14). Compound **14** was obtained from **6** and cyclohexylamine according to the procedure described for **7** and was isolated as a white semisolid (214 mg, 92% yield). ¹H NMR: δ 7.57 (d, $J = 2.2$ Hz, 1H, Ar 3-H), 7.53 (d, $J = 8.5$ Hz, 1H, Ar 6-H), 7.45 (dd, $J = 2.2, 8.5$ Hz, 1H, Ar 5-H), 7.36 (d, $J = 8.5$ Hz, 2H, Ar' 3,5-H), 7.19 (d, $J = 8.5$ Hz, 2H, Ar' 2,6-H), 3.83 (m, 1H, N-CH), 2.29 (s, 3H, CH₃), 1.94 (m, 2H, cyclohex), 1.78 (m, 2H, cyclohex), 1.66 (m, 1H, cyclohex), 1.36 (m, 5H, cyclohex). HPLC: 65% CH₃CN-H₂O, R_t 31.8 min (100%); 85% CH₃OH-H₂O, R_t 8.8 min (100%). TLC: 4:1 EtOAc-Hex, R_f 0.71; 10% MeOH-CHCl₃, R_f 0.72. HREIMS: m/z 461.0834 (calcd for C₂₃H₂₂³⁵Cl₃N₃O, 461.0828).

N-(Morpholin-4-yl)-5-(4-chlorophenyl)-1-(2,4-dichlorophenyl)-4-methyl-1H-pyrazole-3-carboxamide (15). Compound **15** was obtained from **6** and *N*-aminomorpholine according to the procedure described for **7** and was isolated as a white foam (186 mg, 78% yield); mp 235.3–236.2 °C (literature³⁵ mp 247–249 °C). ¹H NMR: δ 7.57 (d, $J = 2.2$ Hz, 1H, Ar 3-H), 7.54 (d, $J = 8.5$ Hz, 1H, Ar 6-H), 7.46 (dd, $J = 2.2, 8.5$ Hz, 1H, Ar 5-H), 7.37 (d, $J = 8.5$ Hz, 2H, Ar' 3,5-H), 7.20 (d, $J = 8.5, 2H$, Ar' 2,6-H), 3.80 (br t, $J = 4.7$ Hz, 4H, N-CH₂), 2.90 (br t, $J = 4.6$ Hz, 4H, O-CH₂), 2.31 (s, 3H, CH₃). HPLC: 70% CH₃CN-H₂O, R_t 4.5 min (100%); 85% CH₃OH-H₂O, R_t 3.6 min (100%). TLC: 30:1 EtOAc-Hex, R_f 0.39; 20% MeOH-CHCl₃, R_f 0.78. HREIMS: m/z 464.0581 (calcd for C₂₁H₁₉³⁵Cl₃N₄O₂, 464.0574).

N-Hydroxy-5-(4-chlorophenyl)-1-(2,4-dichlorophenyl)-4-methyl-1H-pyrazole-3-carboxamide (16). The di-HCl salt of hydroxamic acid (76 mg, 1.09 mmol), triethylamine (500 μ L, 3.59 mmol), and 95% EtOH (5 mL) was cooled to 0 °C under argon and treated dropwise over 5 min with a solution of **6** (218.6 mg, 0.55 mmol) in CH₂Cl₂ (5 mL). The solution was allowed to warm slowly to 25 °C under Ar and stirred for an additional 2 h. The reaction was quenched by addition of 10 mL of H₂O. The organic layer was washed with 2 \times 20 mL of 1 N HCl. The combined aqueous layers were back-extracted with CH₂Cl₂, and the combined CH₂Cl₂ layers were washed

with saturated aqueous NaHCO₃. The aqueous layer was back-extracted with CH₂Cl₂, and the combined CH₂Cl₂ layers were dried over Na₂SO₄. The CH₂Cl₂ was evaporated in vacuo, yielding a brown foam. Flash chromatography (2:3 EtOAc-hexanes) yielded the product as a white foam (144 mg, 73% yield); mp 187.6–188.7 °C. ¹H NMR: δ 7.55 (d, $J = 2.2$ Hz, 1H, Ar 3-H), 7.51 (d, $J = 8.5$ Hz, 1H, Ar 6-H), 7.43 (dd, $J = 2.2, 8.5$ Hz, 1H, Ar 5-H), 7.36 (d, $J = 8.5$ Hz, 2H, Ar' 3,5-H), 7.18 (d, $J = 8.5$ Hz, 2H, Ar' 2,6-H), 2.29 (s, 3H, CH₃). HPLC: 65% CH₃CN-H₂O, R_t 3.6 min (100%); 80% CH₃OH-H₂O, R_t 5.1 min (100%). TLC: 7:1 EtOAc-Hex, R_f 0.51; 20% MeOH-CHCl₃, R_f 0.67. HRFABMS: m/z 396.0082 (calcd for [M + H] C₁₇H₁₃³⁵Cl₃N₃O₂, 396.0073).

N-(2-Hydroxyethyl)-5-(4-chlorophenyl)-1-(2,4-dichlorophenyl)-4-methyl-1H-pyrazole-3-carboxamide (17). Compound **17** was obtained from **6** and 2-aminoethanol according to the procedure described for **7** and was isolated as a colorless oil (196 mg, 88% yield). ¹H NMR: δ 7.57 (d, $J = 2.2$ Hz, 1H, Ar 3-H), 7.52 (d, $J = 8.5$ Hz, 1H, Ar 6-H), 7.44 (dd, $J = 2.2, 8.5$ Hz, 1H, Ar 5-H), 7.36 (d, $J = 8.5$ Hz, 2H, Ar' 3,5-H), 7.19 (d, $J = 8.5$ Hz, 2H, Ar' 2,6-H), 3.69 (t, $J = 5.8$ Hz, 2H, N-CH₂-CH₂-OH), 3.49 (t, $J = 5.8$ Hz, 2H, N-CH₂-CH₂-OH), 2.30 (s, 3H, CH₃). HPLC: 70% CH₃CN-H₂O, R_t 3.9 min (100%); 80% CH₃OH-H₂O, R_t 6.3 min (100%). TLC: 10:1 EtOAc-Hex, R_f 0.43; 20% MeOH-CHCl₃, R_f 0.66. HREIMS: m/z 405.0200 (calcd for [M - H₂O] C₁₉H₁₄³⁵Cl₃N₃O, 405.0202).

N-(3-Hydroxypropyl)-5-(4-chlorophenyl)-1-(2,4-dichlorophenyl)-4-methyl-1H-pyrazole-3-carboxamide (18). Compound **18** was obtained from **6** and 3-amino-1-propanol according to the procedure described for **7** and was isolated as a colorless oil (208 mg, 92% yield). ¹H NMR: δ 7.56 (d, $J = 2.2$ Hz, 1H, Ar 3-H), 7.52 (d, $J = 8.5$ Hz, 1H, Ar 6-H), 7.44 (dd, $J = 2.2, 8.5$ Hz, 1H, Ar 5-H), 7.36 (d, $J = 8.5$ Hz, 2H, Ar' 3,5-H), 7.19 (d, $J = 8.5$ Hz, 2H, Ar' 2,6-H), 3.64 (t, $J = 6.2$ Hz, 2H, N-CH₂-CH₂-CH₂-OH), 3.46 (t, $J = 6.8$ Hz, 2H, N-CH₂-CH₂-CH₂-OH), 2.30 (s, 3H, CH₃), 1.81 (p, $J = 6.5$ Hz, 2H, N-CH₂-CH₂-CH₂-OH). HPLC: 70% CH₃CN-H₂O, R_t 4.4 min (100%); 80% CH₃OH-H₂O, R_t 6.9 min (100%). TLC: 10:1 EtOAc-Hex, R_f 0.42; 20% MeOH-CHCl₃, R_f 0.66. HREIMS: m/z 437.0469 (calcd for C₂₀H₁₈³⁵Cl₃N₃O₂, 437.0465).

N-(4-Hydroxybutyl)-5-(4-chlorophenyl)-1-(2,4-dichlorophenyl)-4-methyl-1H-pyrazole-3-carboxamide (19). Compound **19** was obtained from **6** and 4-amino-1-butanol according to the procedure described for **7** and was isolated as a white semisolid (202 mg, 86% yield). ¹H NMR: δ 7.56 (d, $J = 2.2$ Hz, 1H, Ar 3-H), 7.52 (d, $J = 8.5$ Hz, 1H, Ar 6-H), 7.44 (dd, $J = 2.2, 8.5$ Hz, 1H, Ar 5-H), 7.36 (d, $J = 8.5$ Hz, 2H, Ar' 3,5-H), 7.19 (d, $J = 8.5$ Hz, 2H, Ar' 2,6-H), 3.58 (t, $J = 6.2$ Hz, 2H, N-CH₂-CH₂-CH₂-CH₂-OH), 3.38 (t, $J = 6.8$ Hz, 2H, N-CH₂-CH₂-CH₂-CH₂-OH), 2.30 (s, 3H, CH₃), 1.62 (m, 4H, N-CH₂-(CH₂)₂-CH₂-OH). HPLC: 65% CH₃CN-H₂O, R_t 4.2 min (100%); 80% CH₃OH-H₂O, R_t 7.3 min (100%). TLC: 30:1 EtOAc-Hex, R_f 0.41; 20% MeOH-CHCl₃, R_f 0.65. HREIMS: m/z 451.0626 (calcd for C₂₁H₂₀³⁵Cl₃N₃O₂, 451.0621).

(S)-(+)-N-(2-Hydroxy-1-methylethyl)-5-(4-chlorophenyl)-1-(2,4-dichlorophenyl)-4-methyl-1H-pyrazole-3-carboxamide (20). Compound **20** was obtained from **6** and (S)-(+)-2-amino-1-propanol according to the procedure described for **7** and was isolated as a white semisolid (200 mg, 90% yield). [α]_D²⁰ +8.8° (c 0.08, CHCl₃). ¹H NMR: δ 7.57 (d, $J = 2.2$ Hz, 1H, Ar 3-H), 7.53 (d, $J = 8.5$ Hz, 1H, Ar 6-H), 7.45 (dd, $J = 2.2, 8.5$ Hz, 1H, Ar 5-H), 7.36 (d, $J = 8.5$ Hz, 2H, Ar' 3,5-H), 7.19 (d, $J = 8.5$ Hz, 2H, Ar' 2,6-H), 4.16 (m, 1H, N-CH-(CH₃)-CH₂-OH), 3.58 (d, $J = 5.2$ Hz, 2H, N-CH-(CH₃)-CH₂-OH), 2.30 (s, 3H, CH₃), 1.23 (d, $J = 6.8$ Hz, 3H, N-CH-(CH₃)-CH₂-OH). HPLC: 75% CH₃CN-H₂O, R_t 3.8 min (100%); 80% CH₃OH-H₂O, R_t 7.5 min (100%). TLC: 10:1 EtOAc-Hex, R_f 0.49; 20% MeOH-CHCl₃, R_f 0.72. HREIMS: m/z 437.0481 (calcd for C₂₀H₁₈³⁵Cl₃N₃O₂, 437.0465).

(R)-(-)-N-(2-Hydroxy-1-methylethyl)-5-(4-chlorophenyl)-1-(2,4-dichlorophenyl)-4-methyl-1H-pyrazole-3-carboxamide (21). Compound **21** was obtained from **6** and (R)-(-)-2-amino-1-propanol according to the procedure described for **7** and was isolated as a white semisolid (196 mg, 88% yield).

$[\alpha]_D^{20}$ -3.4° (*c* 0.09, CHCl_3). $^1\text{H NMR}$: δ 7.57 (d, $J = 2.2$ Hz, 1H, Ar 3-H), 7.53 (d, $J = 8.5$ Hz, 1H, Ar 6-H), 7.45 (dd, $J = 2.2, 8.5$ Hz, 1H, Ar 5-H), 7.36 (d, $J = 8.5$ Hz, 2H, Ar' 3,5-H), 7.19 (d, $J = 8.5$ Hz, 2H, Ar' 2,6-H), 4.16 (m, 1H, N-CH-(CH₃)-CH₂-OH), 3.58 (d, $J = 5.3$ Hz, 2H, N-CH-(CH₃)-CH₂-OH), 2.30 (s, 3H, CH₃), 1.23 (d, $J = 6.8$ Hz, 3H, N-CH-(CH₃)-CH₂-OH). HPLC: 75% $\text{CH}_3\text{CN}-\text{H}_2\text{O}$, R_t 3.8 min (100%); 80% $\text{CH}_3\text{OH}-\text{H}_2\text{O}$, R_t 7.6 min (100%). TLC: 10:1 EtOAc-Hex, R_f 0.53; 20% MeOH- CHCl_3 , R_f 0.72. HREIMS: m/z 437.0458 (calcd for $\text{C}_{20}\text{H}_{18}^{35}\text{Cl}_3\text{N}_3\text{O}_2$, 437.0465).

5-(4-Chlorophenyl)-1-(2,4-dichlorophenyl)-4-methyl-1H-pyrazole-3-carbohydrazide (22). Compound **22** was obtained from **6** and the di-HCl salt of hydrazine according to the procedure described for **16** and was isolated as a white semisolid (97 mg, 51% yield). $^1\text{H NMR}$: δ 7.51 (d, $J = 2.2$ Hz, 1H, Ar 3-H), 7.50 (d, $J = 8.5$ Hz, 1H, Ar 6-H), 7.41 (dd, $J = 2.2, 8.5$ Hz, 1H, Ar 5-H), 7.33 (d, $J = 8.5$ Hz, 2H, Ar' 3,5-H), 7.16 (d, $J = 8.5$ Hz, 2H, Ar' 2,6-H), 2.28 (s, 3H, CH₃). HPLC: 60% $\text{CH}_3\text{CN}-\text{H}_2\text{O}$, R_t 6.0 min (98%); 80% $\text{CH}_3\text{OH}-\text{H}_2\text{O}$, R_t 6.5 min (96%). TLC: 30:1 EtOAc-Hex, R_f 0.49; 20% MeOH- CHCl_3 , R_f 0.70. HREIMS: m/z 394.0150 (calcd for $\text{C}_{17}\text{H}_{13}^{35}\text{Cl}_3\text{N}_4\text{O}$, 394.0155).

N-Methyl-5-(4-chlorophenyl)-1-(2,4-dichlorophenyl)-4-methyl-1H-pyrazole-3-carbohydrazide (23). Compound **23** was obtained from **6** and methylhydrazine according to the procedure described for **7** and was isolated as a white solid (184 mg, 90% yield); mp 163.9–166.1 °C. $^1\text{H NMR}$: δ 7.57 (br s, 1H, Ar 3-H), 7.45 (br d, $J = 8.5$ Hz, 1H, Ar 6-H), 7.40 (dd, $J = 2.1, 8.5$ Hz, 1H, Ar 5-H), 7.35 (br d, $J = 8.2$ Hz, 2H, Ar' 3,5-H), 7.19 (d, $J = 8.2$ Hz, 2H, Ar' 2,6-H), 3.39 (s, 3H, N-CH₃), 2.14 (s, 3H, CH₃). HPLC: 60% $\text{CH}_3\text{CN}-\text{H}_2\text{O}$, R_t 5.6 min (99%); 80% $\text{CH}_3\text{OH}-\text{H}_2\text{O}$, R_t 5.5 min (100%). TLC: 30:1 EtOAc-Hex, R_f 0.33; 20% MeOH- CHCl_3 , R_f 0.71. HREIMS: m/z 408.0307 (calcd for $\text{C}_{18}\text{H}_{15}^{35}\text{Cl}_3\text{N}_4\text{O}$, 408.0311).

N-Ethyl-5-(4-chlorophenyl)-1-(2,4-dichlorophenyl)-4-methyl-1H-pyrazole-3-carbohydrazide (24). Compound **24** was obtained from **6** and the di-HCl salt of ethylhydrazine according to the procedure described for **16** and was isolated as a white semisolid (115 mg, 56% yield). $^1\text{H NMR}$: δ 7.57 (br s, 1H, Ar 3-H), 7.41 (br s, 2H, Ar 6-H, Ar 5-H), 7.35 (br d, $J = 8.4$ Hz, 2H, Ar' 3,5-H), 7.19 (d, $J = 8.4$ Hz, 2H, Ar' 2,6-H), 3.74 (q, $J = 6.8$ Hz, 2H, N-CH₂-CH₃), 2.15 (s, 3H, CH₃), 1.26 (t, $J = 6.8$ Hz, 3H, N-CH₂-CH₃). HPLC: 60% $\text{CH}_3\text{CN}-\text{H}_2\text{O}$, R_t 7.8 min (98%); 80% $\text{CH}_3\text{OH}-\text{H}_2\text{O}$, R_t 7.2 min (100%). TLC: 30:1 EtOAc-Hex, R_f 0.46; 10% MeOH- CHCl_3 , R_f 0.44. HREIMS: m/z 422.0473 (calcd for $\text{C}_{19}\text{H}_{17}^{35}\text{Cl}_3\text{N}_4\text{O}$, 422.0468).

N-(1-Propyl)-5-(4-chlorophenyl)-1-(2,4-dichlorophenyl)-4-methyl-1H-pyrazole-3-carbohydrazide (25). Compound **25** was obtained from **6** and the di-HCl salt of 1-propylhydrazine according to the procedure described for **16** and was isolated as a white foam (137 mg, 62% yield); mp 126.7–128.5 °C. $^1\text{H NMR}$: δ 7.61 (br s, 1H, Ar 3-H), 7.43 (br s, 2H, Ar 6-H, Ar 5-H), 7.37 (br d, $J = 8.4$ Hz, 2H, Ar' 3,5-H), 7.20 (d, $J = 8.4$ Hz, 2H, Ar' 2,6-H), 3.68 (t, $J = 7.1$ Hz, 2H, N-CH₂-CH₂-CH₃), 2.14 (s, 3H, CH₃), 1.76 (m, 2H, N-CH₂-CH₂-CH₃), 0.99 (t, $J = 7.3$ Hz, 1H, N-CH₂-CH₂-CH₃), 0.83 (t, $J = 7.4$ Hz, 2H, N-CH₂-CH₂-CH₃). HPLC: 75% $\text{CH}_3\text{CN}-\text{H}_2\text{O}$, R_t 5.5 min (100%); 82% $\text{CH}_3\text{OH}-\text{H}_2\text{O}$, R_t 5.1 min (100%). TLC: 10:1 EtOAc-Hex, R_f 0.42; 10% MeOH- CHCl_3 , R_f 0.41. HREIMS: m/z 436.0625 (calcd for $\text{C}_{20}\text{H}_{19}^{35}\text{Cl}_3\text{N}_4\text{O}$, 436.0624).

N-(1-Butyl)-5-(4-chlorophenyl)-1-(2,4-dichlorophenyl)-4-methyl-1H-pyrazole-3-carbohydrazide (26). Compound **26** was obtained from **6** and the di-HCl salt of 1-butylhydrazine according to the procedure described for **16** and was isolated as a white semisolid (136 mg, 62% yield). $^1\text{H NMR}$: δ 7.58 (br s, 1H, Ar 3-H), 7.41 (br s, 2H, Ar 6-H, Ar 5-H), 7.36 (br d, $J = 8.4$ Hz, 2H, Ar' 3,5-H), 7.19 (d, $J = 8.4$ Hz, 2H, Ar' 2,6-H), 3.72 (m, 1.33H, N-CH₂-CH₂-CH₂-CH₃), 3.35 (m, 0.67H, N-CH₂'-CH₂-CH₂-CH₃), 2.29 (s, 1H, CH₃), 2.14 (s, 2H, CH₃), 1.71 (m, 1.33H, N-CH₂-CH₂-CH₂-CH₃), 1.57 (m, 0.67H, N-CH₂-CH₂'-CH₂-CH₃), 1.40 (m, 0.67H, N-CH₂-CH₂-CH₂'-CH₃), 1.27 (m, 1.33H, N-CH₂-CH₂-CH₂-CH₃), 0.95 (t, $J = 7.3$ Hz, 2H, N-CH₂-CH₂-CH₂-CH₃), 0.84 (t, $J = 7.4$ Hz, 1H, N-CH₂-CH₂-CH₂-CH₃). HPLC: 75% $\text{CH}_3\text{CN}-$

H_2O , R_t 8.3 min (100%); 82% $\text{CH}_3\text{OH}-\text{H}_2\text{O}$, R_t 6.3 min (100%). TLC: 10:1 EtOAc-Hex, R_f 0.47; 10% MeOH- CHCl_3 , R_f 0.42. HREIMS: m/z 450.0770 (calcd for $\text{C}_{21}\text{H}_{21}^{35}\text{Cl}_3\text{N}_4\text{O}$, 450.0781).

N-(2-Methylpropyl)-5-(4-chlorophenyl)-1-(2,4-dichlorophenyl)-4-methyl-1H-pyrazole-3-carbohydrazide (27). Compound **27** was obtained from **6** and the di-HCl salt of 2-methylpropylhydrazine according to the procedure described for **16** and was isolated as a white foam (132 mg, 60% yield). $^1\text{H NMR}$ (DMSO-*d*₆, 300 MHz): δ 7.81 (d, $J = 2.2$ Hz, 1H, Ar 3-H), 7.61 (d, $J = 8.5$ Hz, 1H, Ar 6-H), 7.54 (dd, $J = 2.2, 8.5$ Hz, 1H, Ar 5-H), 7.45 (d, $J = 8.5$ Hz, 2H, Ar' 3,5-H), 7.22 (d, $J = 8.5$ Hz, 2H, Ar' 2,6-H), 5.06 (br s, 0.67H, NH-CH₂-CH-(CH₃)₂), 4.94 (br s, 0.33H, NH-CH₂-CH-(CH₃)₂), 3.49 (br d, $J = 5.3$ Hz, 1.5H, N-CH₂-CH-(CH₃)₂), 3.40 (d, $J = 7.4$ Hz, 0.5H, N-CH₂'-CH-(CH₃)₂), 2.08 (m, 1H, N-CH₂-CH-(CH₃)₂), 2.05 (s, 3H, CH₃), 0.89 (d, $J = 6.6$ Hz, 2H, N-CH₂-CH-(CH₃)₂), 0.75 (d, $J = 6.7$ Hz, 4H, N-CH₂-CH-(CH₃)₂). HPLC: 75% $\text{CH}_3\text{CN}-\text{H}_2\text{O}$, R_t 6.5 min (100%); 82% $\text{CH}_3\text{OH}-\text{H}_2\text{O}$, R_t 6.0 min (100%). TLC: 10:1 EtOAc-Hex, R_f 0.47; 20% MeOH- CHCl_3 , R_f 0.78. HREIMS: m/z 450.0779 (calcd for $\text{C}_{21}\text{H}_{21}^{35}\text{Cl}_3\text{N}_4\text{O}$, 450.0781).

Solvent-Dependent NMR

solvent	isomer (ratio) ^a	CH ₂ (ppm)	(CH ₃) ₂ (ppm)
CDCl ₃	major (3.6)	3.69	0.85
	minor (1.0)	3.54	0.99
pyridine- <i>d</i> ₅	major (2.4)	3.93	0.90
	minor (1.0)	3.79	1.00
DMSO- <i>d</i> ₆	major (2.0)	3.49	0.75
	minor (1.0)	3.40	0.89
MeOH- <i>d</i> ₄	major (1.9)	3.62	0.83
	minor (1.0)	3.54	0.98

^a Ratios were taken of the geminal dimethyl protons, calculated from their integration areas.

Receptor Binding Assays. 1. Rat Membrane Assay. For the competition assays utilizing rat brain membrane preparations, male CD rats (Charles River Laboratories, Raleigh, NC) weighing 220–225 g were sacrificed. The whole brains were quickly removed and placed into a 55 mL Potter-Elvehjem glass homogenizer tube maintained on ice. Alternatively, the brains were placed on dry ice and subsequently frozen at -70°C until processing. The tissue was subjected to a homogenization and centrifugation procedure described previously⁶ to yield the final membrane preparation used in the binding assay. Total protein concentration of the resuspended membrane pellet was determined by a dye-binding assay commercially available from Biorad Laboratories (Hercules, CA). Aliquots of the membrane preparation were stored at -70°C until use.

Compounds **7–27** were evaluated for their ability to compete with the binding of [³H]**2** or [³H]**5**. Competing compounds were prepared in buffer consisting of 50 mM Tris-HCl, pH 7.4, 1 mM EDTA, 3 mM MgCl₂, and 0.5% (w/v) bovine serum albumin (BSA) (buffer A). Tritiated compounds were diluted in buffer A to yield concentrations of 7.2 nM for [³H]**2** and 20 nM for [³H]**5** so that addition to the incubation mixture yielded a final concentration in the assay of 0.72 and 2.0 nM, respectively. Unlabeled drug for determination of nonspecific binding (unlabeled **2** in assays using [³H]**2** and unlabeled **5** in assays using [³H]**5**) was at a final concentration of 10 μM.

The competition assays were conducted in a total volume of 0.5 mL in 1.2 mL polypropylene test tubes. The reaction mixtures (in duplicate) consisted of 50 μL of tritiated drug, 50 μL of unlabeled drug dilution, and sufficient buffer A such that a total volume of 0.5 mL was achieved with the addition of brain membrane extract. Duplicate tubes for nonspecific binding and total binding were prepared by adding 50 μL aliquots of the unlabeled compound to be displaced and of buffer A, respectively. An aliquot of brain membrane extract equivalent to 20–25 μg of protein was added to each tube. The final volume of the reaction mixture was brought to a total of 0.5 mL by the addition of buffer A. After they were mixed by vortex, the reaction tubes were incubated at 30 °C for 1 h.

A 96 manifold Brandel (Gaithersburg, MD) cell harvester was prepared by priming approximately 1 L of cold 50 mM

Tris-HCl, pH 7.4, containing 0.1% (w/v) BSA buffer (buffer B) through the harvester. A 96 well shallow well filter plate (GF/C) pretreated for approximately 1 h in buffer B was placed into the cell harvester. After the incubation period was complete, the reaction was terminated by vacuum filtration of the reaction mixture. The reaction tubes were then rinsed with approximately 4 mL of buffer B. After the tubes were rinsed, the filter plate was removed and allowed to dry thoroughly. Approximately 50 μ L of MicroScint 20 liquid scintillation cocktail (Packard; Meriden, CT) was added to each plate well with an automated cocktail dispenser. The plates were sealed and allowed to sit overnight and then counted in a liquid scintillation counter for a statistically appropriate amount of time.

The amount of radiolabel specifically bound in the absence of competing compounds was calculated by subtracting non-specific binding from total binding. The percentage of this specific binding was then calculated for the amount of radiolabel bound in the presence of various concentrations of each competing compound.

The data were then analyzed using GraphPad Prism (GraphPad Software, Inc.; San Diego, CA), which fit the displacement data to a one-binding site model using a goodness-of-fit quantification based on sum of squares and calculated the K_i for the competing compound. The K_i values are presented as means \pm SEM ($n = 2$) in Table 1.

2. CB₂ Assay. The test compounds 7–27 were further evaluated for their ability to bind to the CB₂ cannabinoid receptor (human, CHO-K1). These assays were conducted as described for rat membrane binding assays above using [³H]2 as radioligand. The protein sources were membranes from CHO-K1 cells transfected with the human recombinant CB₂ cannabinoid receptor (Sigma Chemical Co.; St. Louis, MO) at a final assay concentration of 80 pM. The data were analyzed as described above.

3. GTP- γ -[³⁵S] Binding Assay. GTP- γ -[³⁵S] assays of test compounds 7–27 were conducted according to a variation of Sim et al.³³ The reaction mixture consisted of test compound (105 nM–400 μ M), GDP (200 μ M), GTP- γ -[³⁵S] (100 pM), and rat membrane preparation (45 μ g/mL) in a total volume of 0.5 mL of buffer A above. Nonspecific binding was determined in the presence of 100 μ M unlabeled GTP- γ -S, and basal binding was determined in the absence of drug. Duplicate samples were incubated for 1 h at 30 °C, and the bound complex was filtered from the reaction mixture as described previously and counted in a liquid scintillation counter. Specific binding was calculated by subtracting nonspecific binding from total binding and dividing by the total basal binding minus nonspecific binding. Data were analyzed as described above.

In Vitro Pharmacology. Mouse Vas Deferens Assay. Vasa deferentia were obtained from albino MF1 mice weighing 26–44 g. Each tissue was mounted in a 4 mL organ bath at an initial tension of 0.5 g. The baths contained Mg²⁺-free Krebs solution, which was kept at 35 °C and bubbled with 95% O₂ and 5% CO₂. The composition of the Krebs solution was (mM) as follows: NaCl 118.2, KCl 4.75, KH₂PO₄ 1.19, NaHCO₃ 25.0, glucose 11.0, and CaCl₂·6H₂O 2.54. Isometric contractions were evoked by stimulation with 0.5 s trains of three pulses of 110% maximal voltage (train frequency 0.1 Hz; pulse duration 0.5 ms) through a platinum electrode attached to the upper end and a stainless steel electrode attached to the lower end of each bath. Stimuli were generated by a Grass S48 stimulator and then amplified (Med-Lab channel attenuator) and divided to yield separate outputs to eight organ baths (Med-Lab StimuSplitter). Contractions were monitored by computer using a data recording and analysis system (MacLab) that was linked via preamplifiers (Macbridge) to UF1 transducers. After placement in an organ bath, each tissue was subjected to a stimulation-free period of 15 min and then stimulated for 10 min. Tissues were then subjected to alternate periods of stimulation (5 min) and rest (10 min) until consistent twitch amplitudes were obtained. This equilibration procedure was followed by a stimulation-free period of 10 min. Tissues were then stimulated for 10 min after which the stimulator was

switched off and an antagonist or its vehicle added. Thirty minutes later, the first addition of *R*-(+)-3 was made. Additions of *R*-(+)-3 were made cumulatively at 5 min intervals without washout, the tissues being stimulated for the final 2 min of exposure to each concentration of this agonist. Compounds 11–15 were dissolved in DMSO and *R*-(+)-3 in a solution consisting of 50% DMSO and 50% saline. By themselves, these vehicles did not inhibit the twitch response. Drug additions were made in a volume of 10 μ L. Values have been expressed as means and variability as 95% confidence limits. The degree of inhibition of evoked contractions induced by *R*-(+)-3 was calculated in percentage terms by comparing the amplitude of the twitch response after each addition of *R*-(+)-3 with its amplitude immediately before the first addition of this agonist. K_B values for antagonism of *R*-(+)-3 were calculated by substituting a single concentration ratio value into the equation $(x - 1) = B/K_B$, where x (the concentration ratio) is the concentration of *R*-(+)-3 that produced a particular degree of inhibition in the presence of antagonist at a concentration, B , divided by the concentration of *R*-(+)-3 that produced an identical degree of inhibition in the absence of antagonist.³⁶ Values of the concentration ratio and its 95% confidence limits were determined by symmetrical (2 + 2) dose parallel line assays.³⁷ This method was also used to establish whether two point log concentration–response plots deviated significantly from parallelism.

Acknowledgment. The authors acknowledge and appreciate the editorial assistance of Ms. Kathleen G. Ancheta and the NMR expertise of Mr. Gregory S. Bailey and Dr. Jason P. Burgess. The authors also thank Dr. Michael D. Walla, University of South Carolina, for the high-resolution mass spectra and Dr. Clifford George, Laboratory for the Structure of Matter, Naval Research Laboratory, Washington, DC, for the X-ray crystallographic data. This work was supported by the National Institute on Drug Abuse (NIDA) Grant DA-11638 (B.F.T.) and NIDA Grant DA-09789 (R.G.P.).

Supporting Information Available: Full spectrum figures of temperature-dependent NMR of 27. This material is available free of charge via the Internet at <http://pubs.acs.org>.

References

- Gaoni, Y.; Mechoulam, R. Isolation, Structure and Partial Synthesis of an Active Constituent of Hashish. *J. Am. Chem. Soc.* **1964**, *86*, 1646–1647.
- Mechoulam, R.; Shani, A.; Ederly, H.; Grumfeld, Y. Chemical Basis of Hashish Activity. *Science* **1970**, *169*, 611–612.
- Melvin, L. S.; Johnson, M. R.; Harbert, C. A.; Milne, G. M.; Weissman, A. A Cannabinoid Derived Prototypical Analgesic. *J. Med. Chem.* **1984**, *27*, 67–71.
- Estep, K. G.; D'Ambra, T. E.; Olefirowicz, E. M.; Bell, M. R.; Eissenstat, M. A.; Haycock, D. A.; Ward, S. J. Conformationally Restrained Aminoalkylindoles: Potent, Stereoselective Ligands at the Cannabinoid Binding Site. *NIDA Res. Monogr.* **1991**, *105*, 300–301.
- Devane, W. A.; Hanus, L.; Breuer, A.; Pertwee, R. G.; Stevenson, L. A.; Griffin, G.; Gibson, D.; Mandelbaum, A.; Etinger, A.; Mechoulam, R. Isolation and Structure of a Brain Constituent that Binds to the Cannabinoid Receptor. *Science* **1992**, *258*, 1946–1949.
- Devane, W. A.; Dysarz, F. A., III; Johnson, M. R.; Melvin, L. S.; Howlett, A. C. Determination and Characterization of a Cannabinoid Receptor in Rat Brain. *Mol. Pharmacol.* **1988**, *34*, 605–613.
- Herkenham, M.; Lynn, A. B.; Little, M. D.; Johnson, M. R.; Melvin, L. S.; de Costa, B. R.; Rice, K. C. Cannabinoid Receptor Localization in Brain. *Proc. Natl. Acad. Sci. U.S.A.* **1990**, *87*, 1932–1936.
- Matsuda, L. A.; Lolait, S. J.; Brownstein, M. J.; Young, A. C.; Bonner, T. I. Structure of a Cannabinoid Receptor and Functional Expression of the Cloned cDNA. *Nature* **1990**, *346*, 561–564.
- Munro, S.; Thomas, K. L.; Abu-Shaar, M. Molecular Characterization of a Peripheral Receptor for Cannabinoids. *Nature* **1993**, *365*, 61–65.

- (10) Barth, F.; Casellas, P.; Congy, C.; Martinez, S.; Rinaldi, M.; Anne-Archard, G. Preparation of *N*-Piperidino-5-(4-chlorophenyl)-1-(2,4-dichlorophenyl)-4-methylpyrazole-3-carboxamide. Eur. Patent EP-656354, June 7, 1995, pp 1–12.
- (11) Rinaldi-Carmona, M.; Barth, F.; Héaulme, M.; Shire, D.; Calandra, B.; Congy, C.; Martinez, S.; Maruani, J.; Néliat, G.; Caput, D.; Ferrara, P.; Soubrié, P.; Breliere, J. C.; Le Fur, G. SR141716A, a Potent and Selective Antagonist of the Brain Cannabinoid Receptor. *FEBS Lett.* **1994**, *350*, 240–244.
- (12) Abadji, V.; Lin, S.; Taha, G.; Griffin, G.; Stevenson, L. A.; Pertwee, R. G.; Makriyannis, A. (*R*)-Methanandamide: A Chiral Novel Anandamide Possessing Higher Potency and Metabolic Stability. *J. Med. Chem.* **1994**, *37*, 1889–1893.
- (13) Shire, D.; Calandra, B.; Delpech, M.; Dumont, X.; Kaghad, M.; Le Fur, G.; Caput, D.; Ferrara, P. Structural Features of the Central Cannabinoid CB1 Receptor Involved in the Binding of the Specific CB1 Antagonist SR 141716A. *J. Biol. Chem.* **1996**, *271*, 6941–6946.
- (14) Song, Z. H.; Bonner, T. I. A Lysine Residue of the Cannabinoid Receptor is Critical for Receptor Recognition by Several Agonists but Not WIN55212-2. *Mol. Pharmacol.* **1996**, *49*, 891–896.
- (15) Reggio, P. H.; Greer, K. V.; Cox, S. M. The Importance of the Orientation of the C9 Substituent to Cannabinoid Activity. *J. Med. Chem.* **1989**, *32*, 1630–1635.
- (16) Reggio, P. H.; Panu, A. M.; Miles, S. Characterization of a Region of Steric Interference at the Cannabinoid Receptor Using the Active Analogue Approach. *J. Med. Chem.* **1993**, *36*, 1761–1771.
- (17) Reggio, P. H.; Basu-Dutt, S.; Barnett-Norris, J.; Castro, M. T.; Hurst, D. P.; Seltzman, H. H.; Roche, M. J.; Gilliam, A. F.; Thomas, B. F.; Stevenson, L. A.; Pertwee, R. G.; Abood, M. E. The Bioactive Conformation of Aminoalkylindoles at the Cannabinoid CB1 and CB2 Receptors: Insights Gained from (*E*)- and (*Z*)-Naphthylidene Indenes. *J. Med. Chem.* **1998**, *41*, 5177–5187.
- (18) Reggio, P. H. Ligand–Ligand and Ligand–Receptor Approaches to Modeling the Cannabinoid CB1 and CB2 Receptors: Achievements and Challenges. *Curr. Med. Chem.* **1999**, *6*, 665–683.
- (19) Semus, S. F.; Martin, B. R. A Computer-Graphic Investigation into the Pharmacological Role of the THC–Cannabinoid Phenolic Moiety. *Life Sci.* **1990**, *46*, 1781–1785.
- (20) Thomas, B. F.; Compton, D. R.; Martin, B. R.; Semus, S. F. Modeling the Cannabinoid Receptor: A Three-Dimensional Quantitative Structure–Activity Analysis. *Mol. Pharmacol.* **1991**, *40*, 656–665.
- (21) Thomas, B. F.; Adams, I. B.; Mascarella, S. W.; Martin, B. R.; Razdan, R. K. Structure–Activity Analysis of Anandamide Analogues: Relationship to a Cannabinoid Pharmacophore. *J. Med. Chem.* **1996**, *39*, 471–479.
- (22) Tong, W.; Collantes, E. R.; Welsh, W. J.; Berglund, B. A.; Howlett, A. C. Derivation of a Pharmacophore Model for Anandamide Using Constrained Conformational Searching and Comparative Molecular Field Analysis. *J. Med. Chem.* **1998**, *41*, 4207–4215.
- (23) Xie, X. Q.; Eissenstat, M.; Makriyannis, A. Common Cannabimimetic Pharmacophoric Requirements Between Aminoalkyl Indoles and Classical Cannabinoids. *Life Sci.* **1995**, *56*, 1963–1970.
- (24) Nicklaus, M. C.; Milne, G. W. A.; Burke, T. R., Jr. QSAR of Conformationally Flexible Molecules: Comparative Molecular Field Analysis of Protein-Tyrosine Kinase Inhibitors. *J. Comput.-Aided Mol. Des.* **1992**, *6*, 487–504.
- (25) Keimowitz, A. R.; Martin, B. R.; Razdan, R. K.; Crocker, P. J.; Mascarella, S. W.; Thomas, B. F. QSAR Analysis of Δ^8 -THC Analogues: Relationship of Side-Chain Conformation to Cannabinoid Receptor Affinity and Pharmacological Potency. *J. Med. Chem.* **2000**, *43*, 59–70.
- (26) Barth, F.; Casellas, P.; Congy, C.; Martinez, S.; Rinaldi, M. 3-Pyrazolecarboxamide Derivatives Having Cannabinoid Receptor Affinity. Eur. Patent EP-658546, June 21, 1995, pp 1–22.
- (27) Seltzman, H. H.; Carroll, F. I.; Burgess, J. P.; Wyrick, C. D.; Burch, D. F. Tritiation of SR141716 by Metalation-Iodination-Reduction. Tritium-Proton NOE Study. *J. Labelled Compd. Radiopharm.* **2002**, *45*, 59–70.
- (28) Seltzman, H. H.; Carroll, F. I.; Burgess, J. P.; Wyrick, C. D.; Burch, D. F. Synthesis, Spectral Studies, and Tritiation of the Cannabinoid Antagonist SR141716A. *J. Chem. Soc., Chem. Commun.* **1995**, 1549–1550.
- (29) Carpino, L. A.; Santilli, A. A.; Murray, R. W. Oxidative reactions of hydrazines. V. Synthesis of Monobenzyl 1,1-Disubstituted Hydrazines and 2-Amino-2,3-dihydro-1*H*-benz[de]isoquinoline. *J. Am. Chem. Soc.* **1960**, *82*, 2728–2731.
- (30) Ghali, N. I.; Venton, D. L.; Hung, S. C.; Le Breton, G. C. A High-Yielding Synthesis of Monoalkyl Hydrazines. *J. Org. Chem.* **1981**, *46*, 5413–5414.
- (31) Shim, J. Y.; Collantes, E. R.; Welsh, W. J.; Subramaniam, B.; Howlett, A. C.; Eissenstat, M. A.; Ward, S. J. Three-Dimensional Quantitative Structure–Activity Relationship Study of the Cannabimimetic (Aminoalkyl)indoles Using Comparative Molecular Field Analysis. *J. Med. Chem.* **1998**, *41*, 4521–4532.
- (32) Schmetzer, S.; Greenidge, P.; Kovar, K. A.; Schulze-Alexandru, M.; Folkers, G. Structure–Activity Relationships of Cannabinoids: A Joint CoMFA and Pseudoreceptor Modelling Study. *J. Comput.-Aided Mol. Des.* **1997**, *11*, 278–292.
- (33) Sim, L. J.; Hampson, R. E.; Deadwyler, S. A.; Childers, S. R. Effects of Chronic Treatment with Δ^9 -Tetrahydrocannabinol on Cannabinoid-Stimulated [³⁵S]GTP γ S Autoradiography in Rat Brain. *J. Neurosci.* **1996**, *16*, 8057–8066.
- (34) Pertwee, R. G.; Stevenson, L. A.; Elrick, D. B.; Mechoulam, R.; Corbett, A. D. Inhibitory Effects of Certain Enantiomeric Cannabinoids in the Mouse Vas Deferens and the Myenteric Plexus Preparation of Guinea-Pig Small Intestine. *Br. J. Pharmacol.* **1992**, *105*, 980–984.
- (35) Lan, R.; Liu, Q.; Fan, P.; Lin, S.; Fernando, S. R.; McCallion, D.; Pertwee, R.; Makriyannis, A. Structure–Activity Relationships of Pyrazole Derivatives as Cannabinoid Receptor Antagonists. *J. Med. Chem.* **1999**, *42*, 769–776.
- (36) Tallarida, R. J.; Cowan, A.; Adler, M. W. pA₂ and Receptor Differentiation: A Statistical Analysis of Competitive Antagonism. *Life Sci.* **1979**, *25*, 637–654.
- (37) Colquhoun, D. *Lectures on Biostatistics*; Oxford University Press: Oxford, 1971.

JM010498V